

Single-shot readout and relaxation of singlet/triplet states in exchange-coupled ^{31}P electron spins in silicon

Juan P. Dehollain,^{1,2} Juha T. Muhonen,^{1,2} Kuan Y. Tan,^{1,2,*} David N. Jamieson,^{1,3} Andrew S. Dzurak,^{1,2} and Andrea Morello^{1,2,†}

¹Centre for Quantum Computation and Communication Technology

²School of Electrical Engineering and Telecommunications, UNSW Australia, Sydney NSW 2052, Australia

³School of Physics, University of Melbourne, Melbourne, VIC 3010, Australia

(Dated: March 3, 2014)

We present the experimental observation of a large exchange coupling $J \sim 300 \mu\text{eV}$ between two ^{31}P electron spin qubits in silicon. The singlet and triplet states of the coupled spins are monitored in real time by a Single-Electron Transistor, which detects ionization from both energy- and tunnel-rate-dependent processes in the coupled spin system, yielding single-shot readout fidelities above 95%. The triplet to singlet relaxation time $T_1 \sim 1 \text{ ms}$ at zero magnetic field agrees with the theoretical prediction for J -coupled ^{31}P dimers in silicon. The ability to follow the time evolution of the 2-spin state populations at different magnetic fields gives further insight into the dynamics of the coupled donors system, and the role of hyperfine interactions. These results pave the way to the realization of 2-qubit quantum logic gates with spins in silicon, and highlight the necessity to adopt gating schemes compatible with weak J -coupling strengths.

PACS numbers: 03.67.Lx, 71.70.Gm, 76.30.Da, 85.35.Gv

Entangling two-qubit operations, together with single-qubit rotations, form a universal set of quantum logic gates for circuit-based quantum computing [1]. These have been demonstrated in several physical qubit platforms [2], including spins in semiconductors [3–5]. The best qubit coherence times in the solid state have been obtained with spins in isotopically purified group-IV materials such as silicon [6, 7] and carbon [8, 9]. Silicon offers the additional advantage of being the material that underpins all of modern computer hardware, which makes it a very appealing candidate for spin-based quantum technologies [10–12]. The coherent operation of spin-based qubits in Si has been demonstrated in single ^{31}P donor atoms [13, 14] and double quantum dots [15, 16]. Conversely, an entangling quantum logic gate for a pair of spin qubits in silicon is still awaiting experimental demonstration. Several coupling mechanisms can be used for this purpose, including magnets [17] and microwave photons [18], but the simplest coupling for a pair of spins is the exchange interaction J , arising from the overlap of electron wavefunctions [19, 20].

Exchange interaction between pairs of donors in silicon has been observed in bulk spin resonance experiments [21] and, very recently, by electron transport experiments through a donor molecule [22]. However its application to quantum information processing requires the ability to dynamically control it, and to measure the instantaneous quantum state of the qubits. Here we report the time-resolved observation of large exchange coupling $J \sim 300 \mu\text{eV}$ between the electrons of a ^{31}P donor pair. The ^{31}P pair is integrated within a top-gated silicon Single-Electron Transistor (SET) [23] that we employ to perform single-shot readout of the spin singlet ($|S\rangle = (|\uparrow\downarrow\rangle - |\downarrow\uparrow\rangle)/\sqrt{2}$) and triplet ($|T_-\rangle = |\downarrow\downarrow\rangle, |T_0\rangle =$

$(|\uparrow\downarrow\rangle + |\downarrow\uparrow\rangle)/\sqrt{2}, |T_+\rangle = |\uparrow\uparrow\rangle)$ states of the two-electron system. Operating the device at low electron temperatures ($T_{el} = 125 \pm 25 \text{ mK}$) allows us to perform energy-selective readout (E-RO) [24, 25]. In addition we exploit the significant difference in the size of the orbital wavefunctions for $|S\rangle$ and $|T\rangle$ states to demonstrate tunnel-rate-selective readout (TR-RO) [26]. We apply these techniques to measure the $|T\rangle \rightarrow |S\rangle$ relaxation time T_1 , and its dependence on the external magnetic field B .

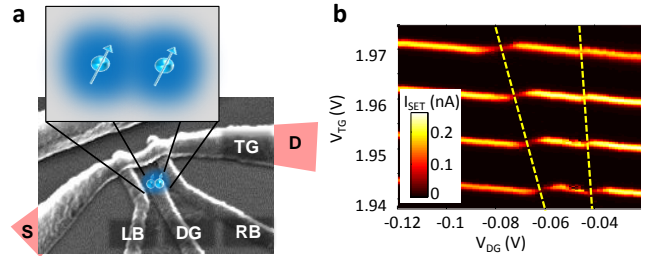


FIG. 1. (Color online) **a**. Scanning electron microscope image of a device similar to the one used in the experiments. The gates TG, LB, RB along with the S, D diffusion regions make up the Single Electron Transistor. Inset shows a sketch of our system of two electron spins with overlapping wavefunctions. **b**. Charge stability diagram, showing two closely spaced charge transitions (dashed lines).

The device described in this work was obtained from the same batch of devices as the one described in detail by Pla *et al.* [13]. A near-intrinsic [001] natural silicon substrate was implanted with phosphorus ions, energy 14 keV [27], using a surface mask to obtain ≈ 3 ions (Poisson statistics) in a $30 \text{ nm} \times 30 \text{ nm}$ window. The donor electrons are tunnel-coupled to the island of a SET, induced under a SiO_2 layer by a stack of Al gates consisting

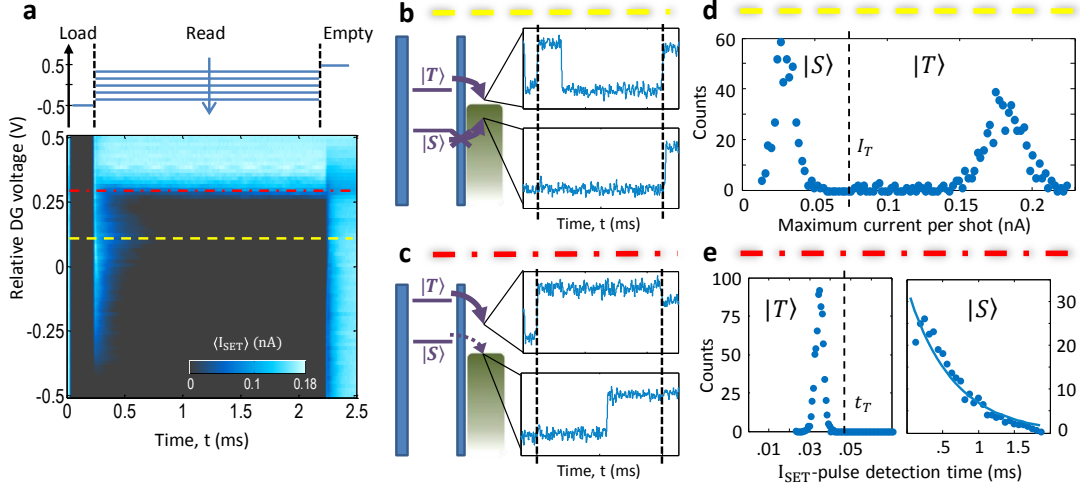


FIG. 2. (Color online) **a.** Three-phase pulse sequence and averaged SET current $\langle I_{\text{SET}} \rangle$, used to identify the DG voltage range where single-shot spin readout can be performed. The dashed and dash-dotted lines identify the appropriate readout-phase voltages to perform energy-selective (E-RO) and tunnel-rate selective (TR-RO) readout, respectively. **b.** E-RO and **c.** TR-RO: Diagrams of the electrochemical potentials μ_S, μ_T relative to the SET Fermi energy E_F ; data plots are examples of readout traces identifying each of the states. **d.** E-RO fidelity measurement: histogram of maximum I_{SET} per shot, with optimal discrimination threshold (vertical dashed line). **e.** TR-RO fidelity measurement: histograms of the detection times of a pulse in I_{SET} during the read-phase. The two histograms are obtained from the same data set, with different bin resolution to distinguish two separate tunneling processes. All histograms are obtained from 1000 single-shot traces, at $B = 0$, with 1 ms load time.

of a top gate (TG) and two (left and right) barrier gates (LB and RB) [23], see Figure 1a. The electrochemical potential μ_D of the donor electrons can be varied using a donor gate (DG) above the implant window. This architecture [28] (Figure 1a) allows for charge detection with very high signal-to-noise ratio [25].

By scanning the TG and DG voltages (V_{TG} and V_{DG}) while measuring the SET current I_{SET} , we obtain the charge stability diagram shown in Figure 1b, where a characteristic pattern of conductance peaks is observed. Ionization of a nearby donor causes the potential of the SET island to shift, generating a discontinuity in the pattern of I_{SET} peaks [25, 28]. The ionization takes place when μ_D is raised above the Fermi energy E_F of the SET island. A first hint of the presence of two closely spaced donors is the presence of two nearby transitions in the charge stability diagram in Figure 1b, indicating that two donors change their charge state at similar values of electrostatic potentials.

With V_{DG} set near a donor charge transition, the device is tuned so the SET will switch between $I_{\text{SET}} = 0$ (Coulomb-blockade) and $I_{\text{SET}} \neq 0$, when the system is neutral or ionized, respectively. In the measurement shown in Figure 2a, we use a 3-level single-shot spin readout sequence [24] consisting of load, read and empty phases. During the read-phase, we measure I_{SET} while varying V_{DG} such that the μ_D goes from higher to lower than E_F . As seen in Figure 2a, there is a well-defined “tail” where excess current occurs at the start of the

read-phase. This indicates the presence of an energy-split pair of electron states. The high-energy electron tunnels out of the donor ($I_{\text{SET}} \neq 0$) shortly after the start of the read-phase, and is replaced by one in the low energy state ($I_{\text{SET}} = 0$ again) thereafter. For a single spin in the presence of a large magnetic field B , the pair of states involved in the process is $|\downarrow\rangle, |\uparrow\rangle$ and the length of the readout “tail” is proportional to their Zeeman splitting $E_Z = \mu_{\uparrow} - \mu_{\downarrow} = g\mu_B B$ [25], where $g \approx 2$ is the Landé g -factor and μ_B is the Bohr magneton. However, the data in Figure 2 was taken at $B = 0$. Therefore we must attribute the observed energy splitting to a different physical mechanism, which acts in the absence of magnetic field. We postulate that the measurement in Figure 2a constitutes the observation of the $|S\rangle$ and $|T\rangle$ states of a pair of ^{31}P donors, split by an exchange interaction $J = \mu_T - \mu_S$, where μ_T and μ_S are the $|T\rangle$ and $|S\rangle$ electrochemical potentials at $B = 0$. To extract the value of J we first convert V_{DG} to a shift in μ , by fitting a Fermi distribution function to the shape of $I_{\text{SET}}(V_{\text{DG}})$ for $0.25 < V_{\text{DG}} < 0.35$ V in the read-phase after the decay of the “tail”, and using the value $T_{\text{el}} = 125 \pm 25$ mK (measured separately) to calibrate the energy scale. Then, the length of the readout “tail” $\Delta V_{\text{DG}} = 0.6 \pm 0.1$ V can be converted into the value of $J = 345 \pm 100$ μeV . This value of J is expected to correspond to donors $\lesssim 8$ nm apart [19, 20, 22].

We perform E-RO in the region indicated by a dashed line in Figure 2a, where $\mu_S < E_F < \mu_T$. In analogy

with the single-spin case [24, 25], the excited state $|T\rangle$ is identified by a pulse of current at the beginning of the read-phase, while $|S\rangle$ keeps $I_{\text{SET}} = 0$ (see Figure 2b for sample real-time readout traces). We estimate the E-RO fidelities using the histogram of maximum current per shot on Figure 2d, with the method described in [25], from which we extract readout fidelities above 95%, with an optimal current threshold $I_T = 0.07$ nA.

Tuning the device to the region indicated by the dash-dot line in Figure 2a, the single-shot readout traces reveal two distinct tunnel-out processes (shown in Figure 2e): A slow process with a tunnel time ≈ 0.9 ms, and a faster process for which the tunnel time is shorter than the rise-time $\approx 35 \mu\text{s}$ of the amplifier chain (see Figure 2c for sample traces). The observation of two very distinct tunnel rates reinforces the interpretation that we are observing the spin states of a J -coupled donor pair. The $|T\rangle$ state must correspond to an excited 2-electron orbital, with a more extended wavefunction [29] that results in stronger tunnel coupling to the nearby SET island. This tunnel rate asymmetry allows us to perform single-shot TR-RO [26] by setting a time threshold (t_T) and declaring that each readout event with tunnel-out time $< t_T$ is a $|T\rangle$ state, and a $|S\rangle$ otherwise (Figure 2e). A statistical analysis of this measurement method reveals a TR-RO readout fidelity $\approx 97\%$, for an optimal $t_T = 44 \mu\text{s}$.

We measure the $|T\rangle$ to $|S\rangle$ relaxation time, T_1 , by taking repeated E-RO traces as a function of the duration τ_w of the load phase, and calculating the probability $P_T(\tau_w)$ of measuring a $|T\rangle$ state (see Figure 3). By fitting the data in Figure 3b with the function $P_T(\tau_w) = P_T(0) \exp(-\tau_w/T_1)$ we extract $T_1 = 1.7 \pm 0.1$ ms. This value agrees well with the $|T\rangle \rightarrow |S\rangle$ relaxation times predicted by Borhani and Hu [30] specifically for ^{31}P donor pairs in Si in the presence of an exchange interaction $J \sim 300 \mu\text{eV}$, providing yet another argument to claim that we observed a J -coupled donor pair. The electron-nuclear hyperfine coupling A (assumed $\ll J$) mixes the J -split $|S\rangle, |T\rangle$ states and provides a new channel for spin-lattice relaxation which is ~ 3 orders of magnitude faster than a single-spin flip at an equivalent value of the Zeeman splitting ($E_Z \approx 300 \mu\text{eV}$ corresponds to $B \approx 2.5$ T on a single spin, where $T_1 \approx 1$ s [25]). The $|T\rangle \rightarrow |S\rangle$ relaxation is predicted to slow down at lower J , giving $T_1 \gg 1$ s for $J \sim 1 \mu\text{eV}$. For $J < A = 117 \text{ MHz} \approx 0.5 \mu\text{eV}$ this relaxation channel becomes suppressed. Therefore our measurements clearly indicate that 2-qubit coupling schemes which do not require large values of J [31, 32] will have the additional benefit of preserving the long spin lifetime of the individual qubits.

The near-unity value of $P_T(0) = 0.91 \pm 0.03$ in Figure 3b indicates that the system is preferentially initialized in $|T\rangle$, as expected from the faster tunnel rate into that state. By performing relaxation measurements in the TR-RO regime, we can follow in real time the evolution of the state populations after the loading of the $|T\rangle$

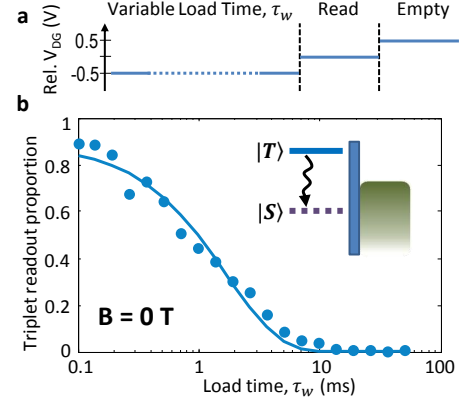


FIG. 3. (Color online) **a.** Gate pulsing scheme for spin relaxation measurements. **b.** $|T\rangle \rightarrow |S\rangle$ relaxation measurement at $B = 0$, using E-RO method (see inset).

state. For these measurements we consider three detection thresholds: fast tunneling events ($t < 44 \mu\text{s}$), slow tunneling events ($44 \mu\text{s} < t < 2$ ms) and no tunneling events within the readout phase (> 2 ms). An intriguing observation is that, at $B = 0$, the sum of the $|S\rangle$ and $|T\rangle$ detection probabilities as a function of load time τ_w is not constant, but exhibits a dip for $\tau_w \sim 1 - 10$ ms (Figure 4a). This indicates that there are intermediate states with extremely low tunnel probability. We suggest that such “shelving states” are the $|T_-\rangle$ and $|T_+\rangle$ states, which at $B = 0$ can be mixed with $|T_0\rangle$ by the Overhauser field from the surrounding nuclear spin bath (in this case, the 4.7% natural abundance of ^{29}Si). To simulate this effect in our relaxation measurements, we designed the following model of rate equations:

$$\begin{aligned} dT_+/d\tau_w &= \Gamma_{T_{\text{mix}}}T_0 - (\Gamma_{T_{\text{mix}}} + \Gamma_{T \rightarrow S})T_+ \\ dT_0/d\tau_w &= \Gamma_{T_{\text{mix}}}(T_+ + T_-) - (2\Gamma_{T_{\text{mix}}} + \Gamma_{T \rightarrow S})T_0 \\ dT_-/d\tau_w &= \Gamma_{T_{\text{mix}}}T_0 - (\Gamma_{T_{\text{mix}}} + \Gamma_{T \rightarrow S})T_- \\ dS/d\tau_w &= \Gamma_{T \rightarrow S}(T_+ + T_0 + T_-) \end{aligned} \quad (1)$$

Here T_0 , T_- , T_+ , S are the populations of the corresponding states, τ_w is the wait time at the load-phase, $\Gamma_{T_{\text{mix}}}$ is the rate of mixing of the $|T\rangle$ states, and $\Gamma_{T \rightarrow S} \equiv 1/T_1$ is the $|T\rangle$ to $|S\rangle$ relaxation rate. We further assume that the tunnel rate of $|T_-\rangle$ and $|T_+\rangle$ is 0, i.e., no tunnel-out signal is obtained if the system is found in those states at the start of the read-phase. We include the parameters $\alpha_{T_0} \equiv T_0|_{\tau_w=0}$ and $\alpha_S \equiv S|_{\tau_w=\infty}$ ($\in [0, 1]$) that multiply the corresponding populations to account for initialization and measurement imperfections. A least-squares numerical fit to the data yields $\Gamma_{T_{\text{mix}}}^{-1} = 6.7 \pm 1.8$ ms, $\Gamma_{T \rightarrow S}^{-1} = 8.7 \pm 1.0$ ms, $\alpha_{T_0} = 0.94 \pm 0.05$, and $\alpha_S = 0.95 \pm 0.05$. The calculated population curves are plotted in Figure 4a, and show good agreement with the data. We attribute the difference between $\Gamma_{T \rightarrow S}^{-1}$ extracted here and T_1 from Figure 3 (both at $B = 0$) to a change in J caused by a different

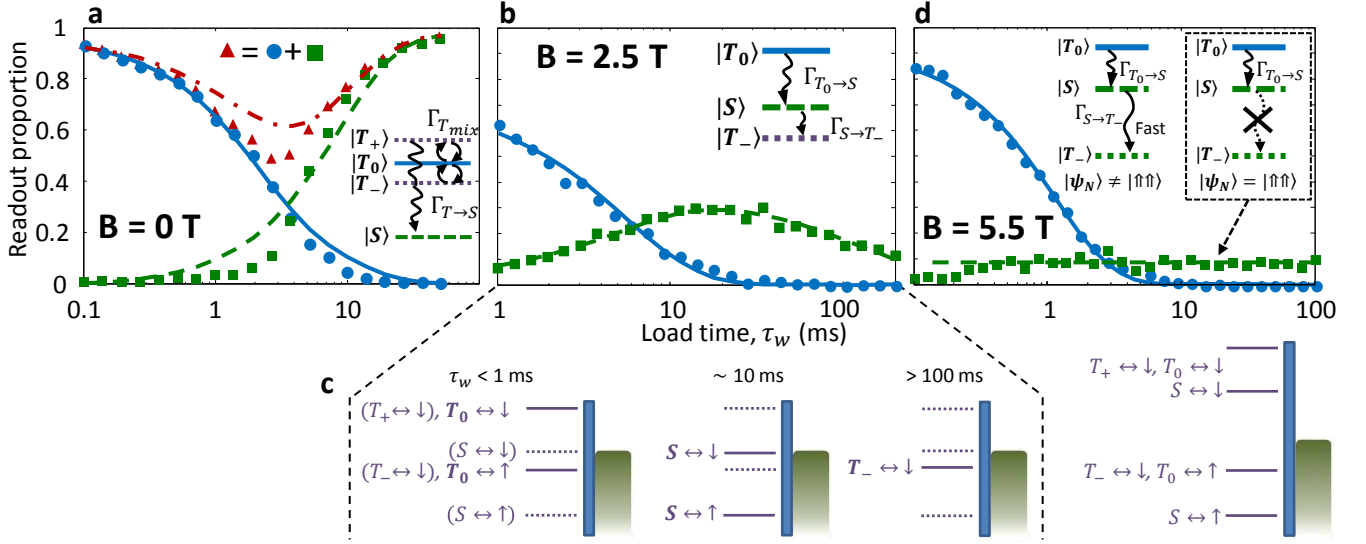


FIG. 4. (Color online) Spin relaxation in different B -field regimes. Dots: fraction of fast tunneling events (using the TR-RO threshold) identified as T_0 . Squares: slow tunneling events, identified as S , excluding those with no observed tunneling in the read-phase. **a.** Spin relaxation at $B = 0$. Solid lines are fits to the model in Equation 1. The triangles correspond to $T_0 + S$. **b.** $B = 2.5$ T, where $E_Z \gtrsim J$ and both $\Gamma_{S \rightarrow T_-}$ and $\Gamma_{T_0 \rightarrow S}$ can be observed. Solid lines are fits to Equation 2. **c.** Diagrams of electrochemical potentials at the resonance between 1- and 2-electron states as indicated. Solid lines and bold letters indicate the most populated states at the indicated wait times (states in brackets and dotted lines are the least populated). **d.** At $B = 5.5$ T, $E_Z \gg J$ and $\Gamma_{S \rightarrow T_-}$ becomes too fast to resolve. Solid line: fit to Equation 2. The long-time plateau of S is due to spin selection rules where relaxation from $|S\rangle$ to $|T_- \rangle$ is forbidden when $|\psi_N\rangle = |\uparrow\uparrow\rangle$ (see text). The lowest diagram shows the electrochemical potentials at the read-phase.

electrostatic tuning of the device. Conversely, we do not have a satisfactory explanation for why the tunnel rates should differ between the $|T\rangle$ states, and we intend to study this problem in more detail in the near future.

Applying a magnetic field B splits the $|T\rangle$ states by the Zeeman energy $E_Z = g\mu_B B$. On the basis of the value of J extracted from the data in Figure 2a, we expect $E_Z > J$ for $B \gtrsim 2.5$ T. By setting $\mu_S < E_F < \mu_{T_-}$ we observed no significant B -dependence of T_1 (data not shown). The nearly constant T_1 for $B < 2.5$ T further reinforces our inference that the system loads preferentially in the $|T_0\rangle$ state, whereas $|T_+\rangle$, $|T_-\rangle$ have negligible tunnel probabilities. This is because the $|T\rangle \rightarrow |S\rangle$ relaxation rate depends strongly on $E_T - E_S$ [30], which is B -independent for $|T_0\rangle$ but B -dependent for $|T_+\rangle$, $|T_-\rangle$ [33].

At fields where $E_Z \gtrsim J$, we use a combination of E-RO and TR-RO to map out the population evolution of $|T_0\rangle$, $|S\rangle$ and $|T_-\rangle$. Figure 4b shows a measurement at $B = 2.5$ T. As τ_w increases, the relaxation proceeds sequentially from $|T_0\rangle$ to $|S\rangle$ to $|T_-\rangle$ (we neglect the single-spin $|T_0\rangle \rightarrow |T_-\rangle$ relaxation channel, for which $\Gamma^{-1} \approx 1$ s at 2.5 T [25], and we assume that $|T_+\rangle$ is never loaded). In the $B \neq 0$ regime the mixing between triplets is sup-

pressed and we can modify the rate equation model as:

$$\begin{aligned} dT_0/d\tau_w &= -\Gamma_{T_0 \rightarrow S} T_0 \\ dS/d\tau_w &= \Gamma_{T_0 \rightarrow S} T_0 - \Gamma_{S \rightarrow T_-} S \\ dT_-/d\tau_w &= \Gamma_{S \rightarrow T_-} S \end{aligned} \quad (2)$$

This model fits the data in Figure 4b with $\Gamma_{T_0 \rightarrow S}^{-1} = 5.4 \pm 0.4$ ms, $\Gamma_{S \rightarrow T_-}^{-1} = 130 \pm 70$ ms, $\alpha_{T_0} = 0.69 \pm 0.29$, and $\alpha_S = 0.30 \pm 0.12$. Here the rates $\Gamma_{T_0 \rightarrow S}$ and $\Gamma_{S \rightarrow T_-}$ are easily resolved because they differ by over an order of magnitude, resulting in a $|S\rangle$ population that first increases ($|T_0\rangle \rightarrow |S\rangle$) then decreases ($|S\rangle \rightarrow |T_-\rangle$).

When $B \gtrsim 4$ T, $\Gamma_{S \rightarrow T_-}$ becomes the fastest rate, and at $B = 5.5$ T (Figure 4d) only $\Gamma_{T_0 \rightarrow S}^{-1} = 1.16 \pm 0.06$ ms, with $\alpha_{T_0} = 0.88 \pm 0.03$, can be reliably extracted from the data. Interestingly, we observe a constant population of $|S\rangle$ for $\tau_w \gtrsim 1$ ms. This is again consistent with the spin relaxation mechanism described by the theory of Borhani and Hu [30], where the hyperfine interaction A mixes states having the same total value of the electron (m_e) and nuclear (m_N) spin quantum number. The transition $|S\rangle \rightarrow |T_-\rangle$ yields $\Delta m_e = -1$, thus requires $\Delta m_N = +1$. Therefore the transition becomes forbidden if the ^{31}P nuclei are in the state $|\psi_N\rangle = |\uparrow\uparrow\rangle$, resulting in a long-time plateau of S with height depending on the probability that $|\psi_N\rangle = |\uparrow\uparrow\rangle$. $|\psi_N\rangle$ is unknown and uncontrolled in this experiment, but we may assume that the nuclei randomly populate all possible states over the

time necessary to acquire a set of data as in Figure 4. At $B < 2.5$ T this selection rule does not affect the experiment, because $|S\rangle$ is the ground state and mixes with $|T_0\rangle$ for any $|\psi_N\rangle$.

The time-resolved observation of singlet and triplet states of an exchange-coupled ^{31}P donor pair reported here provides a physical basis for the construction of large-scale donor-based quantum computer architectures [11]. The short $|T\rangle \leftrightarrow |S\rangle$ relaxation times $T_1 \sim 1$ ms in this experiment arise from the interplay of a large exchange coupling $J \approx 300 \mu\text{eV}$ with the hyperfine interaction $A = 117 \text{ MHz} \approx 0.5 \mu\text{eV}$. Therefore, our results indicate that the best regime to operate J -mediated 2-qubit logic gates is where $J \lesssim A$, as described in recent proposals [31, 32].

We acknowledge discussions with M. House, T. Watson and X. Hu. This research was funded by the Australian Research Council Centre of Excellence for Quantum Computation and Communication Technology (project number CE110001027) and the US Army Research Office (W911NF-13-1-0024). We acknowledge support from the Australian National Fabrication Facility.

* Present address: QCD Labs, COMP Centre of Excellence, Department of Applied Physics, Aalto University, 00076 Aalto, Finland

† a.morello@unsw.edu.au

- [1] C. H. Bennett and D. P. DiVincenzo, *Nature* **404**, 247 (2000).
- [2] T. D. Ladd, F. Jelezko, R. Laflamme, Y. Nakamura, C. Monroe, and J. L. O'Brien, *Nature* **464**, 45 (2010).
- [3] J. R. Petta, A. C. Johnson, J. M. Taylor, E. A. Laird, A. Yacoby, M. D. Lukin, C. M. Marcus, M. P. Hanson, and A. C. Gossard, *Science* **309**, 2180 (2005).
- [4] M. D. Shulman, O. E. Dial, S. P. Harvey, H. Bluhm, V. Umansky, and A. Yacoby, *Science* **336**, 202 (2012).
- [5] K. C. Nowack, M. Shafiei, M. Laforest, G. E. D. K. Prawiroatmodjo, L. R. Schreiber, C. Reichl, W. Wegscheider, and L. M. K. Vandersypen, *Science* **333**, 1269 (2011).
- [6] A. M. Tyryshkin, S. Tojo, J. J. L. Morton, H. Riemann, N. V. Abrosimov, P. Becker, H.-J. Pohl, T. Schenkel, M. L. W. Thewalt, K. M. Itoh, and S. A. Lyon, *Nature Materials* **11**, 143 (2012).
- [7] M. Steger, K. Saeedi, M. L. W. Thewalt, J. J. L. Morton, H. Riemann, N. V. Abrosimov, P. Becker, and H.-J. Pohl, *Science* **336**, 1280 (2012).
- [8] G. Balasubramanian *et al.*, *Nature Mater.* **8**, 383 (2009).
- [9] P. C. Maurer *et al.*, *Science* **336**, 1283 (2012).
- [10] B. E. Kane, *Nature* **393**, 133 (1998).
- [11] L. Hollenberg, A. Greentree, A. Fowler, and C. Wellard, *Physical Review B* **74**, 045311 (2006).
- [12] F. A. Zwanenburger, A. S. Dzurak, A. Morello, M. Y. Simmons, L. C. L. Hollenberg, G. Klimeck, S. Rogge, S. N. Coppersmith, and M. A. Eriksson, *Reviews of Modern Physics* **85**, 961 (2013).
- [13] J. J. Pla, K. Y. Tan, J. P. Dehollain, W. H. Lim, J. J. L. Morton, D. N. Jamieson, A. S. Dzurak, and A. Morello, *Nature* **489**, 541 (2012).
- [14] J. J. Pla, K. Y. Tan, J. P. Dehollain, W. H. Lim, J. J. L. Morton, F. A. Zwanenburger, D. N. Jamieson, A. S. Dzurak, and A. Morello, *Nature* **496**, 334 (2013).
- [15] B. M. Maune *et al.*, *Nature* **481**, 344 (2012).
- [16] D. Kim, Z. Shi, C. Simmons, D. Ward, J. Prance, T. S. Koh, J. K. Gamble, D. Savage, M. Lagally, M. Friesen, *et al.*, [arXiv:1401.4416](https://arxiv.org/abs/1401.4416) (2014).
- [17] L. Trifunovic, F. L. Pedrocchi, and D. Loss, *Phys. Rev. X* **3**, 041023 (2013).
- [18] X. Hu, Y.-x. Liu, and F. Nori, *Phys. Rev. B* **86**, 035314 (2012).
- [19] B. Koiller, X. Hu, and S. Das Sarma, *Phys. Rev. Lett.* **88**, 027903 (2001).
- [20] C. J. Wellard, L. C. L. Hollenberg, F. Parisoli, L. M. Kettle, H.-S. Goan, J. A. L. McIntosh, and D. N. Jamieson, *Phys. Rev. B* **68**, 195209 (2003).
- [21] D. Jérôme and J. M. Winter, *Phys. Rev.* **134**, A1001 (1964).
- [22] M. F. Gonzalez-Zalba, A. Saraiva, D. Heiss, M. J. Calderón, B. Koiller, and A. J. Ferguson, [arXiv:1312.4589](https://arxiv.org/abs/1312.4589) (2013).
- [23] S. Angus, A. Ferguson, A. Dzurak, and R. Clark, *Nano Letters* **7**, 2051 (2007).
- [24] J. Elzerman, R. Hanson, L. van Beveren, B. Witkamp, L. Vandersypen, and L. Kouwenhoven, *Nature* **430**, 431 (2004).
- [25] A. Morello *et al.*, *Nature* **467**, 687 (2010).
- [26] R. Hanson, L. van Beveren, I. Vink, J. Elzerman, W. Naber, F. Koppens, L. Kouwenhoven, and L. Vandersypen, *Physical Review Letters* **94**, 196802 (2005).
- [27] D. Jamieson, C. Yang, T. Hopf, S. Hearne, C. Pakes, S. Prawer, M. Mitic, E. Gauja, S. Andresen, F. Hudson, *et al.*, *Applied Physics Letters* **86**, 202101 (2005).
- [28] A. Morello, C. C. Escott, H. Huebl, L. H. Willems van Beveren, L. C. L. Hollenberg, D. N. Jamieson, A. S. Dzurak, and R. G. Clark, *Physical Review B* **80**, 81307 (2009).
- [29] L. P. Kouwenhoven, D. G. Austing, and S. Tarucha, *Reports on Progress in Physics* **64**, 701 (2001).
- [30] M. Borhani and X. Hu, *Physical Review B* **82**, 241302 (2010).
- [31] R. Kalra, A. Laucht, C. Hill, and A. Morello, [arXiv:1312.2197](https://arxiv.org/abs/1312.2197) (2013).
- [32] V. Srinivasa, H. Xu, and J. M. Taylor, [arXiv:1312.1711](https://arxiv.org/abs/1312.1711) (2013).
- [33] J. R. Prance *et al.*, *Physical Review Letters* **108**, 046808 (2012).